Co-variation of temperature and precipitation in CMIP5 models and satellite observations

Article

Accepted Version

Co-variation of temperature and precipitation in CMIP5 models and satellite observations

Chunlei Liu[1], Richard P. Allan[1] and George J. Huffman[2]

[1] *Department of Meteorology, University of Reading, Reading, UK*

[2] Science Systems and Applications, Inc., and NASA Goddard Space Flight Center, Greenbelt, MD, USA

ABSTRACT

Current variability of precipitation (P) and its response to surface temperature (T) are analysed using coupled (CMIP5) and atmosphere-only (AMIP5) climate model simulations and compared with observational estimates. There is striking agreement between Global Precipitation Climatology Project (GPCP) observed and AMIP5 simulated P anomalies over land both globally and in the tropics suggesting that prescribed sea surface temperature and realistic radiative forcings are sufficient for simulating the interannual variability in continental P. Differences between the observed and simulated P variability over the ocean, originate primarily from the wet tropical regions, in particular the western Pacific, but are reduced slightly after 1995. All datasets show positive responses of P to T globally of around 2 %/K for simulations and 3-4 %/K in GPCP observations but model responses over the tropical oceans are around 3 times smaller than GPCP over the period 1988-2005. The observed anticorrelation between land and ocean P, linked with El Niño Southern Oscillation, is captured by the simulations. All data sets over the tropical ocean show a tendency for wet regions to become wetter and dry regions drier with warming. Over the wet region (≥75% precipitation percentile), the precipitation response is ~13-15%/K for GPCP and ~5%/K for models while trends in P are 2.4%/decade for GPCP, 0.6% /decade for CMIP5 and 0.9%/decade for AMIP5 suggesting that models are underestimating the precipitation responses or a deficiency exists in the satellite datasets.

1. Introduction

The change in the global water cycle in a warming climate is a primary concern of society [*Meehl et al.*, 2007]. Model projections have indicated significant water cycle changes, with the intensification of extreme precipitation, the already wet areas getting wetter and the dry areas getting drier [*Allan et al.,* 2010; *Seager and Naik*, 2011; *Noake et al.,* 2012]. There is a robust physical basis for expecting precipitation (P) to increase in the global mean and in particular for regions of moisture convergence as surface temperature (T) rises, relating to energy and moisture balance constraints [*Held and Soden,* 2006; *Mitchell et al.*, 1987; *Muller and O'Gorman*, 2011; *Seager and Naik*, 2011]. Using multi-satellite observations, *Liu and Allan* [2012] assessed the consistency of the observed variability in P, and it was found that there is good agreement among data sets including GPCP (Global Precipitation Climatology Project) [*Adler et al.*, 2008], SSM/I (Special Sensor Microwave Imager) [*Wentz and Spencer,* 1998; *Vila et al.,* 2010], AMSRE (Advanced Microwave Scanning Radiometer - Earth Observing System) [*Lobl*, 2001], and TMI (Tropical Rainfall Measuring Mission (TRMM) Microwave Imager) over the tropical ocean and between GPCP and the TRMM 3B42 product [*Huffman et al.,* 2007] over the tropical land (expected since both data sets use very similar gauge analyses and methodologies). Comparing climate model simulations with observations over the tropical oceans, *Allan et al.* [2010] found that the wet region (highest 30% of monthly precipitation values) is becoming wetter and the dry region (lowest 70% of monthly precipitation values) is becoming drier. However, results are sensitive to data sets and time period [*Liu and Allan,* 2012].

In the present study, we assess the current changes in global P simulated by historical scenarios from phase 5 of the Coupled Model Intercomparison Project (CMIP5) and the atmosphere-only experiments (AMIP5) which are forced by realistic sea surface temperature (SST) and sea ice and radiative forcings. The aim of the present study is to evaluate how realistic and robust the models are in simulating the recent past, particularly over the satellite microwave measurement era. We assess the consistency and discrepancy between the simulations and the observations which has implications for the confidence in the projections of future climate change.

2. Data sets

We consider three observational data sets in the present study (GPCP, TMI and TRMM 3B42; Table 1). The GPCP is a global blended data set at 2.5^o resolution containing land-based rain-gauges, sounding observations, microwave radiometers and infrared radiances [*Adler et al.*, 2008]. The TMI data set only covers the tropical ocean from 40^{o}N to 40^{o}S at 0.25^o resolution. The TRMM 3B42 covers the area from 50^{o}N to 50^{o}S at 0.25^o resolution including both the land and ocean area but changes in ocean P are not considered realistic [*Liu and Allan,* 2012] because the existing AMSU-B algorithm failed to detect light rain over oceans, particularly in the subtropical highs [*Huffman et al* . 2007]; a corrected version is expected to be available soon. The data over the land region are consistent with GPCP observations. Observed T is the temperature at 2 m from the European Centre for Medium-range Weather Forecasts (ECMWF) INTERIM reanalysis [*Dee et al.*, 2011] accumulated from six hourly 0.25^o data interpolated from the original N128 reduced Gaussian grid (~0.7^o). Blended T from the HadCRUT3 data set [*Brohan et al.*, 2006] is also used for comparison purpose. Ocean (land) points are defined where all four neighbouring grid points are also ocean (land), aggregating from a high resolution (0.25x0.25 degree) land/sea mask; coastal grid points, which may be less reliable in the observational data (e.g. Huffman and Bolvin, 2011), are excluded from the ocean-only and land-only comparisons in both models and observations. Details of the currently available CMIP5 historical experiments (12 models) and the AMIP5 experiments (10 models) and their forcings are at http://cmip-pcmdi.llnl.gov/cmip5/. To ensure equal weighting from each model, we consider only one ensemble member from each CMIP5 and AMIP5 model to form composite CMIP5 and AMIP5 data sets (Table 1).

3. Temperature and precipitation variations

The deseasonalized T and P anomalies from ERA INTERIM, CMIP5, AMIP5 and satellite observations are plotted in Fig. 1. Mean P is also plotted in Fig. S1 and listed in Table S2. The reference period is from 1988-2004 except for the TMI and TRMM data sets (1998-2004). Unlike the AMIP experiment which prescribes observed SST, the CMIP5 T simulations do not follow ERA INTERIM and have a large standard deviation since CMIP5 models generate their own ocean variability. The CMIP5 simulations contain realistic radiative forcings and can simulate cooling after the volcanic eruptions of El Chichón in 1982 and Mount Pinatubo in

1991 that are qualitatively consistent with AMIP5 simulations and observations (e.g. Fig. 1c). The El Niño effect in 1988, 1998, 2005 and the La Niña effect in 1985, 1989, 2008 are clearly seen in the AMIP5 and ERA INTERIM T anomalies (Figs. 1g-1i).

There is striking agreement between observed and AMIP5 simulated P anomalies over land both globally (Fig. 1e; r=0.6) and in the Tropics (30^{o}N -30^{o}S) (Fig. 1k; r=0.7). This suggests that prescribing the observed SST and realistic radiative forcings is sufficient for simulating interannual variability in land P. In general warmer years are associated with negative land P anomalies as noted previously [*Adler et al.*, 2008; *Gu et al.*, 2007] and will be discussed in Section 4.

GPCP displays greater P variation than both CMIP5 and AMIP5 globally (Fig. 1f) (the standard deviation of P from GPCP (~0.03 mm/day) is also higher than the individual models (~0.02 mm/day)) which is determined by the global and tropical oceans (Figs. 1d and 1j), though both AMIP5 and observations show positive phase correlations with T anomalies after 1995. To investigate the origin of these discrepancies, P anomaly differences between the AMIP5 ensemble mean and GPCP are calculated over the tropical ocean (Fig. 2a). The anomaly difference standard deviation (red line in Fig. 2a) is slightly reduced after 1995.

Based on the periods of positive and negative area mean anomaly differences in Fig. 2a, the maps of mean anomaly differences are calculated for all positive (P^+) and negative (P^-) AMIP5 minus GPCP anomaly composites over the period 1988-2008. The difference of $P^+–P^-$ is plotted in Fig. 2b. Regions of positive difference (the west and central south Pacific and western Indian Ocean) display a sign of variation that is consistent with the anomaly differences. This is further confirmed by plotting correlations between the local P anomaly difference time series and that of the tropical ocean mean (Fig. 2c). The regions that appear to contribute most strongly to the changes in AMIP5-GPCP anomaly differences are associated with the largest climatology difference between AMIP5 mean and GPCP P (Fig. 2d).

There are a number of changes to the observed ocean data used in this study which may contribute to the discrepancy discussed above. For GPCP the switch from Outgoing Longwave Radiation (OLR) Precipitation Index (OPI) to Adjusted Geosynchronous Observational Environmental Satellite (GOES) Precipitation Index

(AGPI) in mid-1987 is known to introduce an inhomogeneity in variance. The higher quality of the AGPI is the basis for examining changes starting in 1988 as well as 1979. Subsequent transitions between SSM/I sensors in 1992 and 1995, and a change in aggregating the infrared data in 1996 are considered unlikely to provoke significant differences. As well, the GPCP shifts from low-orbit to geosynchronous-orbit IR data over the Indian Ocean in mid-1998 (Huffman and Bolvin, 2011). Removing the Indian Ocean (20^{o}E-120^{o}E) from the analysis improves the AMIP5-GPCP comparison much less than removing the West Pacific Ocean (Fig. S2b, S3b; Table S3), suggesting that the shift in Indian Ocean IR coverage does not introduce an inhomogeneity. Finally, the source of surface data used in the SST analysis shifts from Comprehensive Ocean-Atmosphere Data Set (COADS) to Global Telecommunications System (GTS) in 1998 (Hurrell et al. 2008), reducing the surface data population available to provide calibration thereafter, but not obviously biasing the results.

Natural changes may also influence the GPCP-AMIP time-series discrepancy. Both models and observational retrievals tend to exhibit different errors for different mean states of the atmosphere and therefore one might anticipate bias changes as the atmosphere changes. For example, the changing character of El Niño Southern Oscillation (ENSO) from an East Pacific (EP) to Central Pacific (CP)-dominated El Nino [Yeh et al., 2009] may influence the statistical comparison of AMIP5 and GPCP since the climate simulation bias is strongest in the west Pacific. Indeed, the CP El Nino years (1990, 1994 and 2004) appear to correspond with negative AMIP5-GPCP in Fig. 2a. A related issue is the shift in the Pacific Decadal Oscillation in the mid-1990's. Changes in volcanic activity may also influence the GPCP-AMIP differences (large volcanic eruptions early in the record in 1982 and 1991) and this is another possibility to explore (e.g. Gu et al. 2007). Additional joint work by modelers and observationalists is needed to explicate the basis for the differences.

Fig. 2e shows the scatter plot of the P anomalies between the AMIP5 mean and GPCP data sets over the tropical ocean, together with fitted lines (thick) over two periods (1988-1995 and 1996-2008). The correlation coefficient is -0.11 for 1988-1995 and is 0.23 over 1996-2008. The fitted lines between individual models and GPCP are also plotted in thin dashed line over these two periods: all models have positive and higher correlations over 1996-2008. The error source is quite complicated and merits further investigation but nevertheless is suggestive of deficiency of the ocean observations prior to the introduction of the SSM/I F13 data in 1995. It is expected that the comparison should be improved using the final version of GPCP 2.2 data [*Huffman and Bolvin*, 2011].

4. Precipitation response to surface temperature variation

Precipitation response to the seasonal and interannual surface temperature variations are displayed in Figs. 3a-3c and quantified in Tables 2 and S1. The relationships from CMIP5 and AMIP5 models are very close over the different regions analysed. For comparison purposes, unless stated otherwise, the data period used from now on is 1988-2005 for CMIP5, AMIP5 and GPCP data sets and from 1998-2008 for the TMI and TRMM 3B42 data sets.

The thick solid fitted lines denote statistically significant correlation (r) between P and T based on the two-tailed test using Pearson critical values at the level of 5% (dashed fitted lines denote correlations are not significant). The degree of freedom of the time series is calculated by first determining the time interval (t_o) between effectively independent samples [*Yang and Tung*, 1998] but additionally assuming $t_o \leq 12$. (assuming that periods separated by 12 or more months are independent).

Over the tropical ocean, the correlations between P and T are all positive. The precipitation change is ~3%/K for CMIP5 and AMIP5 simulations. It is 10%/K for GPCP P and ERA INTERIM T and 7.9 %/K if HadCRUT3 T is used, close to 10.9%/K calculated by *Adler et al.* [2008] using an earlier version of GPCP.

Negative correlations over the tropical land (–3.4 %/K for CMIP5 and –1.9%/K for AMIP5) are similar to GPCP (-3.1 %/K using ERA INTERIM T and -1.2%/K for HadCRUT3 T), but is smaller than TRMM 3B42 (-10 %/K for ERA INTERIM T and -11%/K for HadCRUT3 T) although this is for a short time period and most of the correlations are not statistically significant. Over the globe the GPCP dP/dT is positive and higher than the models (Table 2).

The response over the tropical ocean and the tropical land is of opposite sign (Fig. 3d) for all datasets. The correlations are strong and significant (Table 2) and relate to ENSO [*Gu et al.*, 2007], although monsoons must also play a vital role [*Hsu et al*. 2010]. A similar relationship is also found between the global land and the global ocean (Fig. 3e).

The strong relationship between GPCP and AMIP5 precipitation anomalies over the tropical land (Fig. 3f) is evident for the periods 1979-2008 (r=0.71), 1988-2008 (r=0.75) and 1998-2008 (r=0.74) but is weaker for AMIP5/TRMM 3B42 (r=0.35) over the 1998-2008 period. The agreement between the AMIP5 ensemble mean and GPCP data over tropical and global land is encouraging and suggests a strong control of ocean temperature on land precipitation as noted previously [*Gimeno et al.*, 2010].

5. Responses from wet and dry regions over the tropical ocean

To further understand the source of discrepancy between tropical ocean P anomalies we now analyse the variability in terms of the monthly rainfall intensity distribution. Following *Liu and Allan* [2012], monthly precipitation is divided into percentile bins in ascending order of intensity and the anomaly time series of P averaged over the percentile bin is calculated. The anomaly time series of the area-weighted T over the tropical ocean is also calculated and the linear least square fit gradient, dP/dT, is computed. The percentage change ($dP_{\%}/dT$) is calculated by dividing dP/dT by the mean P for each bin over the reference period of 1988-2004.

The $dP_{\%}/dT$ and $dP_{\%}/dt$ trend over the precipitation percentile bins are plotted in Figs 4a-4b and computed in Table 3. The non-linear scale of precipitation percentile is chosen since the higher percentiles contribute more to overall precipitation. The response is uncertain over the lower percentile bins, but is in general negative, consistent with *Allan et al*. [2010]. The wet region is characterized by positive $dP_{\%}/dT$ in all data sets although the GPCP response is stronger. For $dP_{\%}/dt$, there is no physical reason to anticipate trends in tropical mean P unless there are associated trends in T or radiative forcings [*Andrews et al.*, 2010]. The bin separating the positive and negative responses is around the 75% percentile for both calculations, consistent with previous analysis [*Allan et al.*, 2010].

$dP_{\%}/dT$ relationships over the wet (≥75% precipitation percentile) region are positive and significant for all data sets. For GPCP data over the wet region, the change is 15%/K, around three times the model simulated responses and explains the discrepancy identified for the tropical ocean mean dP/dT discussed in Section 4.

Over the dry region the changes in P from models and GPCP data are quite consistent (~ -6%/K) when ERA INTERIM T is used (Fig. 4a).

The precipitation anomaly time series over the wet and dry regions is plotted in Figs. 4c and 4d. The general trend is positive over the wet region and negative over the dry region despite the reduced trend in T since the 1998 El Niño. The correlations between P over the wet and dry regions are -0.62 and -0.74 for CMIP5 and AMIP5 respectively and are significant. The GPCP variation in dry region P appears inconsistent with the AMIP5 ensemble after 1998 and is suggestive of a change in the sensitivity to light rainfall; the correlation between P over the wet and dry regions is insignificant (-0.12). For GPCP data, the precipitation trend over the wet region is 2.4 %/decade, close to previous estimates by *Allan et al.* [2010] but larger than CMIP5 and AMIP5 responses. Consistent with the tropical ocean mean comparison, correlation between GPCP and AMIP5 P in the wet region is improved after 1995 (r=0.06 over 1988-1995; r=0.72 over 1996-2008). Conversely, over the dry regions of the tropical ocean, agreement between AMIP5 and GPCP data becomes *poorer* after 1995 (r=0.38 over 1988-1995 and r=0.15 over 1996-2008). Over the dry region the CMIP5 and AMIP5 responses are substantially smaller in magnitude than GPCP but all data sets show a drying of the dry regions, though the correlations (r~0.3) are insignificant.

6. Summary

Current changes in precipitation over land and ocean are diagnosed from CMIP5 climate model simulations and compared with blended observations from GPCP and data from the TRMM satellite. Agreement between precipitation anomalies from GPCP and AMIP5 data set over the land (r~0.6) indicates that the atmosphere processes over the land are well represented by simulations including realistic SST and sea-ice changes and radiative forcings. Discrepancies between the observed and simulated tropical ocean P variability is found to originate primarily from the wet regions, in particular the west Pacific, but is reduced for the most recent period (1996-2008). However, differences over the dry regions of the tropical ocean are also evident and show poorer agreement between AMIP5 and GPCP data *after* 1995. This suggests that observed precipitation variability over the ocean is sensitive to changes in the observing system; changes in ENSO character combined with model-satellite bias spatial signature may also influence the AMIP5–GPCP bias and trend differences.

Despite the discrepancies, in all datasets considered, global and tropical ocean precipitation increases robustly with warming although observed responses appear stronger than those from models. Over the time period 1988-2005 the responses are 2.0%/K for CMIP5, 2.3 %/K for AMIP5 and 3-4 %/K for GPCP over the globe. Tropical ocean responses are larger but the responses over the tropical ocean and the tropical land are of opposite sign due to ENSO variability [*Gu et al.*, 2007]. There is a weak negative relationship between P and T over tropical land but the relationship between precipitation over the tropical land and the tropical ocean is strongly negative ($r \leq -0.5$).

The analysis of precipitation change with temperature and with time show positive changes over the high precipitation percentile bins and negative change over the lower precipitation percentile bins, consistent with previous studies [*Lau and Wu*, 2011]. Though the detailed precipitation changes still vary from model to observations and from model to model, the general characteristics of the precipitation variation and responses to the surface temperature variation are consistent. This supports the strong physical basis for expecting increased global precipitation with warmer surface temperatures due to energy constraints [*Allen and Ingram*, 2002] and for anticipating enhanced precipitation minus evaporation patterns due to moisture balance constraints [*Held and Soden*, 2006] and energy constraints [*Muller and O'Gorman*, 2011]. However, further work is required to disentangle fast precipitation responses to radiative forcings from the thermodynamic responses [*Andrews et al.*, 2010; *Ming et al.*, 2010; *Wild et al.*, 2008] and to resolve the discrepancy between current interannual variability in observed and simulated tropical ocean precipitation.

Acknowledgements. This work was undertaken as part of the PAGODA and PREPARE projects funded by the UK Natural Environmental Research Council under grants NE/I006672/1 and NE/G015708/1 and was supported by the National Centre for Earth Observations and the National Centre for Atmospheric Science. GPCP v2.2 data were extracted from http://precip.gsfc.nasa.gov/gpcp_v2.2_data.html, TMI data from ftp.ssmi.com, TRMM 3B42 data from http://mirador.gsfc.nasa.gov/, and CMIP5 and AMIP5 data sets from the

BADC (British Atmospheric Data Centre, http://badc.nerc.ac.uk/home/index.html) and the PCMDI (Program for Climate Model Diagnosis and Intercomparison, http://pcmdi3.llnl.gov/esgcet/home.htm). The scientists involved in the generation of these data sets are sincerely acknowledged. We sincerely thank the two reviewers for their insightful comments which have helped to improve the paper.

7. References

Adler, R.F., G. Gu, G.J. Huffman, J.J. Wang, S. Curtis, and D.T. Bolvin (2008), Relationships between global precipitation and surface temperature on interannual and longer timescales (1979-2006), *J. Geophys. Res.*, *113* (D22104), doi: 10.1029/2008JD010536.

Allan, R. P., B. J. Soden, V. O. John, W. Ingram, and P. Good (2010), Current changes in tropical precipitation, *Environ. Res. Lett.*, 5, 025205, doi:10.1088/1748-9326/5/2/025205.

Allen, M. R. and W. J. Ingram (2002), Constraints on future changes in climate and the hydrologic cycle, *Nature* 419, 224-232.

Andrews, T., P. M. Forster, O. Boucher, N. Bellouin, and A. Jones (2010), Precipitation, radiative forcing and global temperature change, *Geophys Res Lett 37*, L14701, doi:10.1029/2010GL04399.

Brohan, P., J.J. Kennedy, I. Harris, S.F.B. Tett, and P.D. Jones (2006), Uncertainty estimates in regional and global observed temperature changes: a new dataset from 1850, *J. Geophysical Research* **111**, D12106, doi:10.1029/2005JD006548.

Dee, D. P. et al. (2011), The ERA-Interim reanalysis: Configuration and performance of the data assimilation system, *Q.J. Roy. Meteorol. Soc.*, *137*, 553-597. doi:10.1002/qj.828.

Gimeno, L., A. Drumond, R. Nieto, R. M. Trigo, andA. Stohl (2010), On the origin of continental precipitation, *Geophys. Res. Lett*., 37, L13804, doi:10.1029/2010GL043712.

Gu, G., R. F. Adler, G. J. Huffman, and S. Curtis (2007), Tropical rainfall variability on interannual-to-interdecadal and longer time scales derived from the GPCP monthly product, *J. Climate*, *20*, 4033–404.22.

Held, I., and B. J. Soden (2006), Robust responses of the hydrological cycle to global warming. *J. of Climate*, *19(21)*, 5686-99, doi:10.1175/JCLI3990.1.

Hsu, Y. H., C. Chou, and K. Y. Wei (2010), Land–Ocean Asymmetry of Tropical Precipitation Changes in the Mid-Holocene, *J. Climate*, *23*, 4133–4151.

Huffman, G.J., et al. (2007), The TRMM Multisatellite Precipitation Analysis (TMPA): Quasi-Global, Multiyear, Combined-Sensor Precipitation Estimates at Fine Scales, *J. Hydrometeor.* Huffman, G. J., and D. T. Bolvin (2011), GPCP Version 2.2 Combined Precipitation Data Set Documentation (ftp://precip.gsfc.nasa.gov/pub/gpcp-v2.2/doc/V2.2_doc.pdf)

Hurrell, J.W., J.J. Hack, D. Shea, J.M. Caron, J. Roskinski (2008) A new sea surface temperature and sea ice boundary dataset for the Community Atmosphere Model. *J. Climate*, 21, 5145-5153.

Lau, K. M., and H. T. Wu (2011), Climatology and changes in tropical oceanic rainfall characteristics inferred from Tropical Rainfall Measuring Mission (TRMM) data (1998–2009), *J. Geophys. Res.*, *116*, D17111, doi:10.1029/2011JD015827.

Liu, C., and R. P. Allan (2012), Multi-satellite observed responses of precipitation and its extremes to interannual climate variability, *J. Geophys. Res., 117*, D03101, doi:10.1029/2011JD016568, .

Lobl, E. (2001), Joint Advanced Microwave Scanning Radiometer (AMSR) Science Team meeting. *Earth Observer 13(3)*: 3-9.

Meehl, G. et al. (2007), Global climate projections Climate Change 2007: The Physical Science Basis. Contribution of Working Group I to the Fourth Assessment Report of the Intergovernmental Panel on Climate Change ed S Solomon, D Qin, M Manning, Z Chen, M Marquis, K B Averyt, M Tignor and H L Miller (Cambridge: Cambridge University Press) pp 747–845.

Ming, Y., V. Ramaswamy, and G. Persad (2010), Two opposing effects of absorbing aerosols on global mean precipitation, Geophys. Res. Lett., 37, L13701, doi:10.1029/2010GL042895.

Mitchell, J., C. A. Wilson, and W. M. Cunnington (1987), On CO2 climate sensitivity and model dependence of results, *Quart J Roy Meteorol Soc 113*, 293–32.23

Muller, C. J., and P. A. O'Gorman (2011), An energetic perspective on the regional response of precipitation to climate change, *Nature Climate Change 1*, 266-271.

Noake, K., D. Polson, G. Hegerl, and X. Zhang (2012), Changes in seasonal land precipitation during the latter twentieth-century, Geophys. *Res. Lett.*, *39*, L03706, doi:10.1029/2011GL050405.

Seager, R., and N. Naik (2011), A Mechanisms-Based Approach to Detecting Recent Anthropogenic Hydroclimate Change, *J. Clim.*, *25,236-261*.

Vila D., D. R. Ferraro, and H. Semunegus (2010), Improved Global Rainfall Retrieval using the Special Sensor Microwave Imager (SSM/I), *J. Appl. Meteor. Climatol.*, *49*, 1032–1043. doi: 10.1175/2009JAMC2294.1.

Wentz, F. J., and R. W. Spencer (1998), SSM/I Rain Retrievals within a Unified All-Weather Ocean Algorithm, *J. Atmos. Sci*., *55*, 1613-1627.

Wild, M., J. Grieser, and C. Schär (2008), Combined surface solar brightening and increased greenhouse effect support recent intensification of the global land-based hydrological cycle, *Geophys. Res. Lett.,* 35, L17706, doi: 10.1029/2008GL034842.

Yang, H., and K. K. Tung (1998), Water Vapor, Surface Temperature, and the Greenhouse Effect — A Statistical Analysis of Tropical-Mean Data, *J. Clim.*, *11,2686-2697*.

Yeh, S. W., J. S. Kug, B. Dewitte, M. H. Kwon, B. P. Kirtman, and F. F. Jin (2009), El Niño in a changing climate, *Nature* 461, 511-514, doi:10.1038/nature08316

Figure captions

Fig. 1. Temperature and precipitation anomaly time series relative to the reference period of 1988-2004 over the global (a-f) and the tropical (30^oS-30^oN) (g-l) areas except for TMI and TRMM 3B42 from 1998-2004. The black line is ERA INTERIM for temperature (a-c and g-i) and GPCP for precipitation (d-f and j-l). Shaded curves denote the CMIP5 and AMIP5 ensemble mean ± one standard deviation . Five month running means are applied.

Fig. 2. (a) Time series of the area mean P anomaly difference (AMIP5 ensemble mean minus GPCP) over the tropical ocean, together with the five month running mean (thick black line) and the standard deviation over 1979-1995 and 1996-2008 periods (red), (b) the mean difference composite between positive anomaly months and negative anomaly months from 1988-2008 based on (a), (c) the correlation between the local anomaly difference time series and that from (a) over the period of 1988-2008, (d) the P climatology difference between AMIP5 ensemble mean and GPCP over 1988-2008 and (e) scatter plot of tropical ocean P anomalies between AMIP5 ensemble mean and GPCP over 1988-1995 and 1996-2008 periods , together with the fitted lines from AMIP5 ensemble mean and individual models.

Fig. 3. Scatter plot of P and T anomalies (a-c) and P anomalies over the land and the ocean (d-e) from CMIP5/AMIP5 models and satellite-based observations and between AMIP5 and observed P anomalies over tropical land (f). Plotted linear fits are solid where significant at the 95% confidence level.

Fig. 4. The change of tropical ocean precipitation with (a) tropical ocean mean temperature ($dP_{\%}/dT$) and (b) time ($dP_{\%}/dt$) over different precipitation percentile bins and precipitation time series over the wet (c) (≥75% precipitation percentile) and dry (d) (<75% precipitation percentile) regions. Also displayed are CMIP5 and AMIP5 ensemble mean (solid line) ± one standard deviation (shaded area).

Solid symbols highlight significant correlations over the percentile bin and the time series is five month running mean. The seasonal cycle has been removed from all datasets.

Table 1. Data sets and their properties (r1 is the first member of the model run).

Data set	Resolution Lat x Lon	AMIP5 1979-2008 monthly	CMIP5 1979-2005 Monthly
BCC-CSM	2.77^o x 2.81^o		r1
CanESM2	2.77^o x 2.81^o	r1	r1
CCSM4	0.94^o x1.25^o		r1
CNRM-CM5	1.39^o x 1.41^o	r1	r1
CSIRO-Mk3.6	1.85^o x1.88^o		r1
GISS-E2	2.0^o x2.5^o	r1	r3
HadGEM2	1.25^o x1.88^o	r1	r1
INMCM4	1.5^o x 2.0^o	r1	r1
IPSL-CM5A-LR	1.89^o x 3.75^o	r1	r1
MIROC5	1.39^o x 1.41^o	r1	r1
MPI-ESM-LR	1.85^o x1.88^o	r1	
MRI-CGCM3	1.11^o x 1.13^o	r1	r1
NorESM1-M	1.89^o x 2.5^o	r1	r1
GPCP v2.2 1979 – 2010	Combined observed precipitation from satellite and rain gauges. Monthly data, global ocean and land, 2.5^o resolution.		
TMI v4 1997 – present	Monthly data, tropical ocean only (40^oN -40^oS), 0.25^o resolutions.		
TRMM 3B42 v6 1998 – present	Tropical ocean and land (50^oN -50^oS), 0.25^o resolution. (TMI, SSM/I, AMSR), daily data.		
ERA INTERIM 1979 - present	6 hourly, global, 0.25^o resolution.		
HadCRUT3 1979 - 2011	Monthly data, 5^o resolution.		

Table 2. Relationships of dP/dT and dP_{land}/dP_{ocean} over different region and time period. Significant correlation coefficient (r) at the 95% confidence level are marked in bold. Δm is the error range of the gradient m. Values are in the round bracket when HadCRUT3 T is used and values in square bracket are the ranges of m from ensemble members. TMI ocean and TRMM 3B42 land datasets are combined for dP_{land} / dP_{ocean} calculations. The values for each model runs are listed in Table S1.

Data set	Period	dP/dT						dP_{land}/dP_{ocean}			
		Global		Tropical ocean		Tropical land		Global		Tropical	
		m±Δm (%/K)	r	m±Δm (%/K)	r	m±Δm (%/K)	r	m±Δm	r	m±Δm	r
GPCP v2.2	1988-2005	3.8±0.5	**0.48**	10.3±1.0	**0.57**	-3.1±0.9	-0.22	-0.36±0.08	-0.30	-0.81±0.09	**-0.52**
		(3.1±0.5)	(0.43)	(7.9±0.9)	**(0.52)**	(-1.2±1.0)	(-0.08)				
TMI ocean/ TRMM 3B42 land	1998-2008			15.5±1.5	**0.68**	-10.0±1.5	-0.51			-0.97±0.11	**-0.61**
				(17.2±1.5)	**(0.71)**	(-11.1±1.9)	(-0.46)				
CMIP5	1988-2005	2.0±0.04	**0.72**	3.1±0.1	**0.51**	-3.4±0.2	**-0.31**	-1.1±0.03	**-0.52**	-1.6±0.04	**-0.59**
		[0.7 to 2.9]		[1.4 to 4.4]		[-13.4 to 0.6]		[-2.2 to -0.23]		[-3.2 to -0.4]	
AMIP5	1988-2005	2.3±0.06	**0.63**	3.0±0.17	**0.35**	-1.9±0.33	-0.12	-1.2±0.04	**-0.54**	-1.5±0.05	**-0.54**
		[1.6 to 3.6]		[-0.4 to 5.5]		[-7.4 to 0.7]		[-1.9 to -0.7]		[-2.7 to -0.7]	

Table 3. Tropical precipitation change with temperature and time. Correlation (r) is in bold when significant at the 95% confidence level. Values are in the round bracket when HadCRUT3 T is used and values in square bracket are the ranges of m from ensemble members. The T is the area mean over the tropical ocean (30°N -30°S).

Data set	Period	dP_{wet}/dT		dP_{dry}/dT		dP_{wet}/dt		dP_{dry}/t	
		m±Δm (% /K)	r	m±Δm (% /K)	r	m±Δm (%/dec)	r	m±Δm (%/dec)	r
GPCP v2.2	1988-2005	15±1.0 (13±0.8)	**0.71** **(0.75)**	-5.9±3.1 (-11.6±2.6)	-0.13 (-0.30)	2.4±0.32	0.44	-3.5±0.76	-0.30
CMIP5	1988-2005	4.6±0.2 [1.7 to 8.3]	**0.53**	-5.4±0.3 [-13 to 4]	**-0.31**	0.6±0.09 [-0.1 to 1.3]	0.42	-0.5±0.12 [-2.6 to 1.4]	-0.29
AMIP5	1988-2005	5.4±0.3 [1.8 to 8.0]	**0.40**	-6.0±0.5 [-15 to 1.4]	**-0.24**	0.9±0.16 [0.3 to 1.6]	0.36	-1.5±0.28 [-3.7 to 0.2]	-0.35

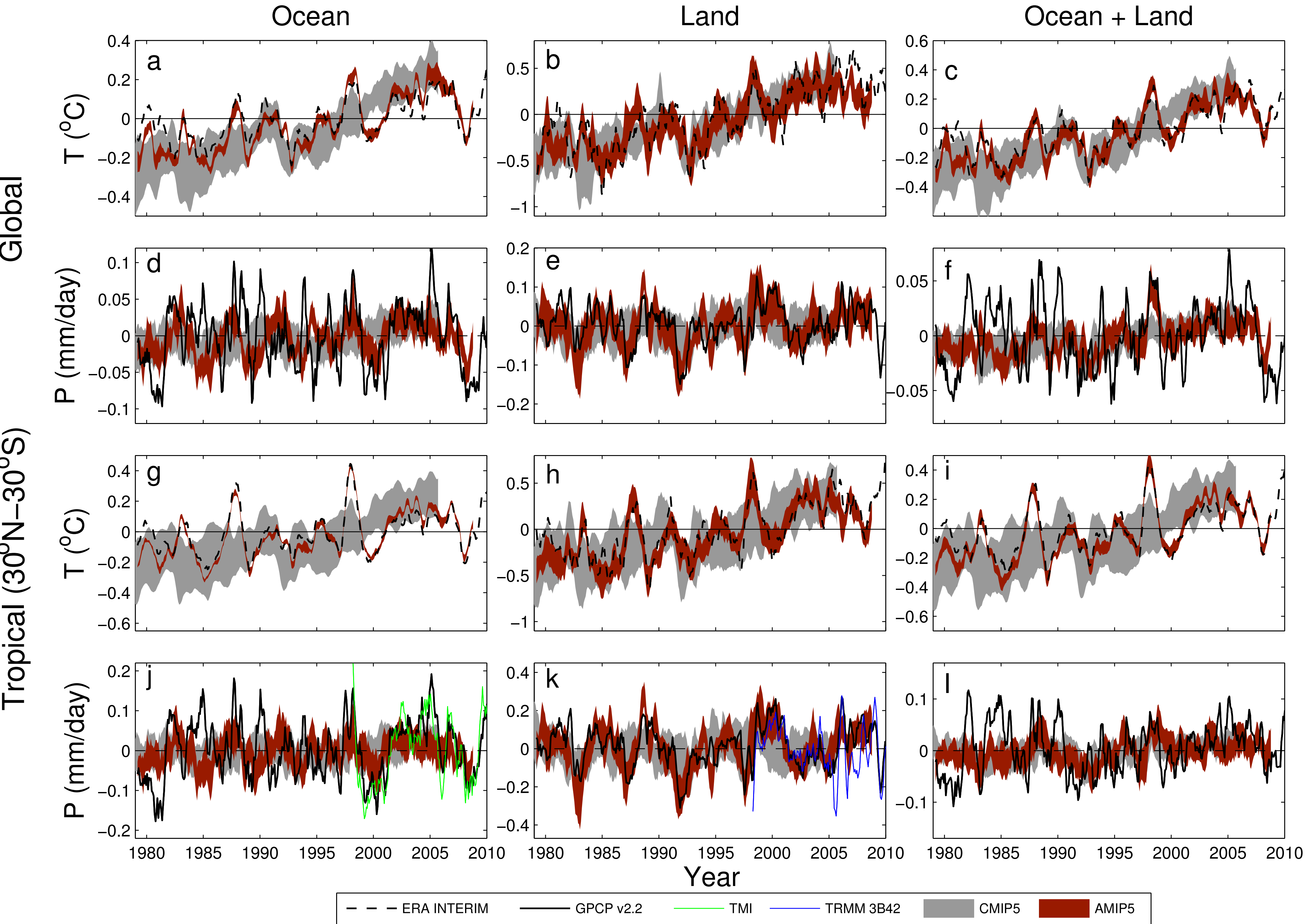

Ocean
Land
Ocean + Land
Global
Tropical (30°N–30°S)
T (°C)
P (mm/day)
a
b
c
d
e
f
g
h
i
j
k
l
Year
1980
1985
1990
1995
2000
2005
2010
ERA INTERIM
GPCP v2.2
TMI
TRMM 3B42
CMIP5
AMIP5

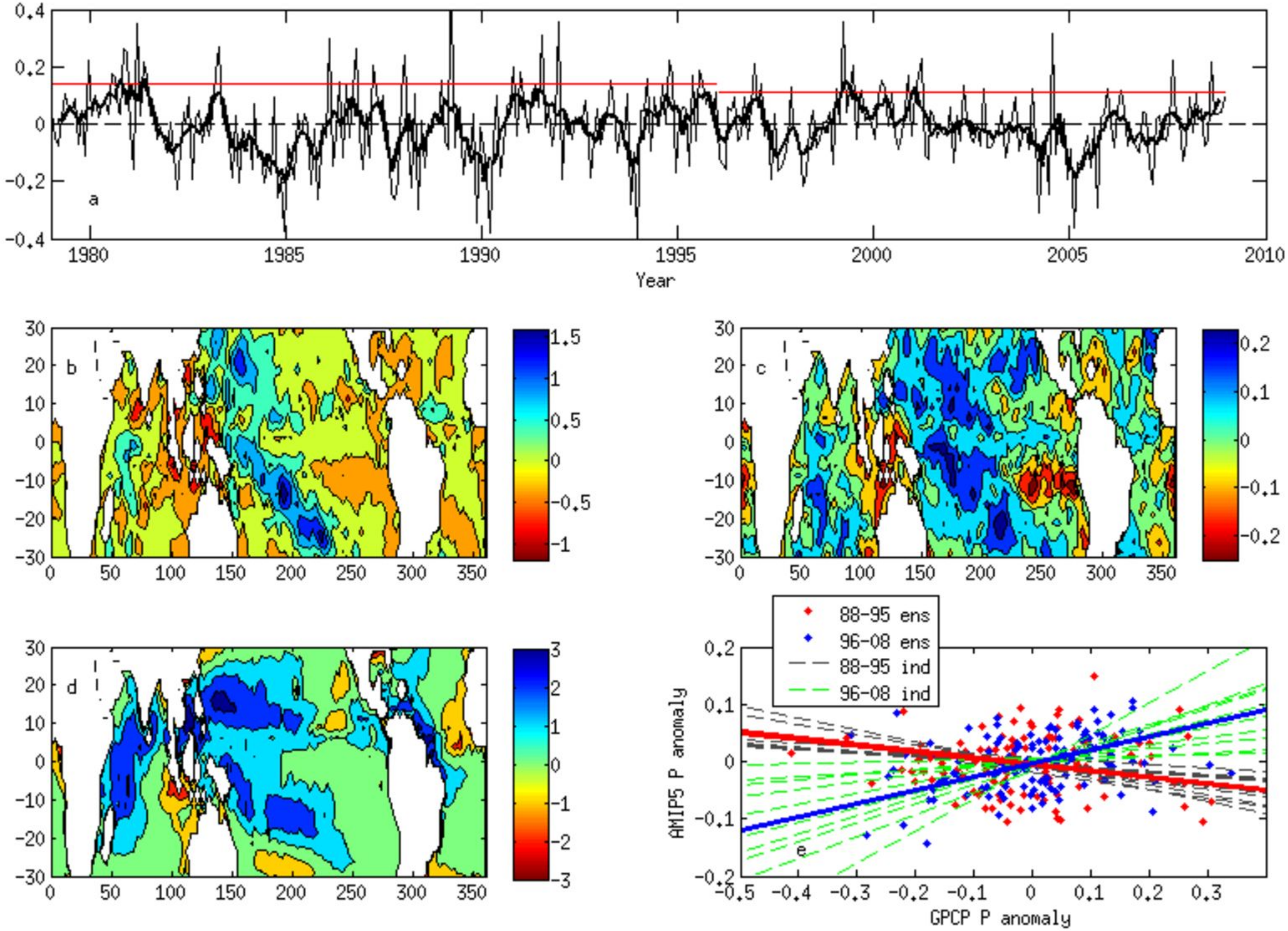

a
Year
b
c
d
e
88-95 ens
96-08 ens
88-95 ind
96-08 ind
AMIP5 P anomaly
GPCP P anomaly

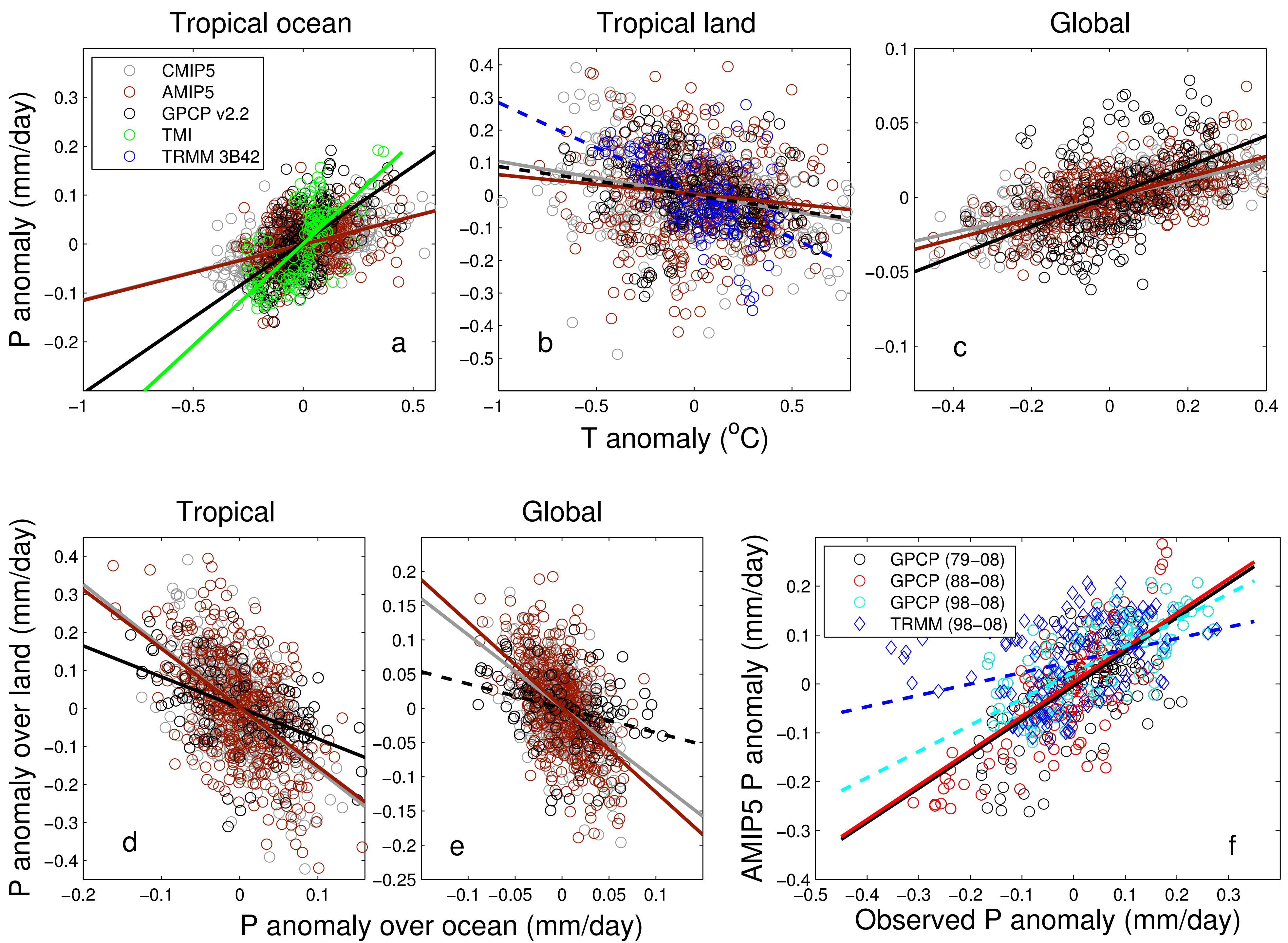

Tropical ocean
Tropical land
Global
CMIP5
AMIP5
GPCP v2.2
TMI
TRMM 3B42
P anomaly (mm/day)
T anomaly (°C)
a
b
c
Tropical
Global
P anomaly over land (mm/day)
P anomaly over ocean (mm/day)
d
e
GPCP (79–08)
GPCP (88–08)
GPCP (98–08)
TRMM (98–08)
AMIP5 P anomaly (mm/day)
Observed P anomaly (mm/day)
f

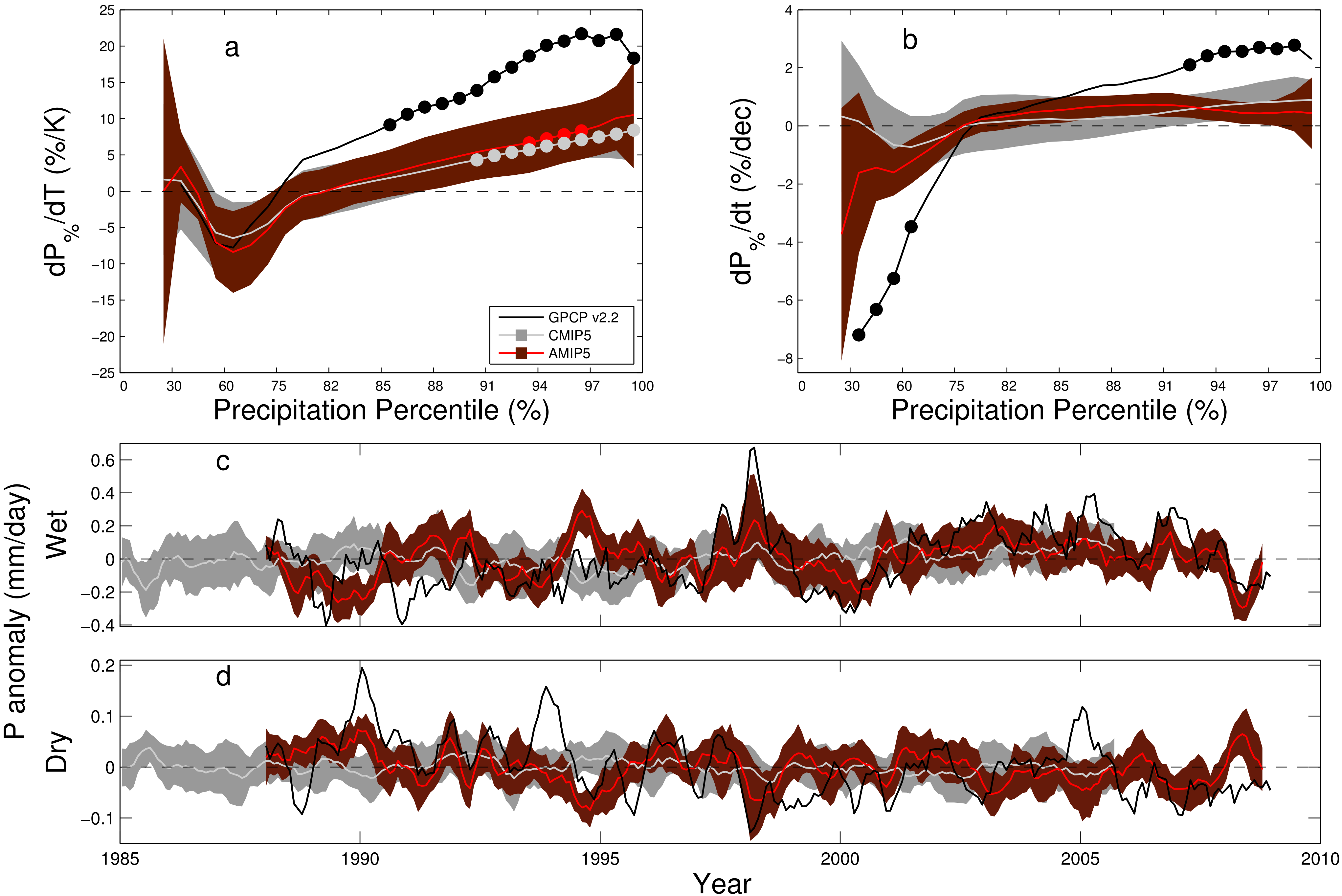

a
b
c
d
GPCP v2.2
CMIP5
AMIP5
dP%/dT (%/K)
dP%/dt (%/dec)
Precipitation Percentile (%)
Precipitation Percentile (%)
P anomaly (mm/day)
Wet
Dry
Year